John S. Latsis
Public Benefit Foundation

RESEARCH PROJECTS 2012

Is the Spili Fault Responsible for the Double Destruction of the Minoan Palace at Phaistos?

Vasiliki Mouslopoulou
Technical University of Crete

Daniel Moraetis
Technical University of Crete

Lucilla Benedetti
CEREGE, CNRS, France

Valery Guillou,
CEREGE, CNRS, France

Dionisis Hristopulos
Technical University of Crete

December 2012

Abstract

This study explores the possible relationship between seismic activity on the Spili Fault in Crete and the double destruction of the Minoan Palace at Phaistos approximately 3750 and 3400 years Before Present (BP). The paleoearthquake activity on the Spili Fault is examined using a novel methodology that combines measurements of *Rare Earth Elements* (REE) and of *in situ cosmogenic* ^{36}Cl on the exhumed fault scarp. Data show that the Spili Fault is active and has generated a minimum of five large-magnitude earthquakes over the last 16000 years. The two most recent events occurred 200 and 400 years ago producing a cumulative displacement of 3.5 meters. The timing of the three older paleoearthquakes is constraint at 8200, 15000 and 16000 years BP with slip sizes of 2.5, 1.20 and 1.80 meters, respectively. The magnitude of the earthquakes that produced the measured co-seismic displacements range from M 6.3-7.3 and the average earthquake recurrence interval on the Spili Fault is about 3500 years. The above data not only suggest that no large-magnitude earthquake was generated by the Spili Fault during the Minoan period but, in contrast, during that period the fault experienced a long phase of seismic quiescence. Hence, our study rejects the hypothesis that there is a link between seismic movement on the Spili Fault and destruction of the Minoan Phaistos, despite the fact that Spili is among the most active faults on Crete. The responsible fault is yet to be identified; here we propose two new candidate faults.

Περίληψη

Αυτή η μελέτη εξετάζει πιθανή συσχέτιση ανάμεσα στην σεισμική δραστηριότητα του ρήγματος του Σπηλίου στην Κρήτη και της διπλής καταστροφής της Μινωϊκής Φαιστού το 1750 και 1400 π.Χ. Η παλαιοσεισμική δραστηριότητα στο ρήγμα του Σπηλίου μελετήθηκε χρησιμοποιώντας μία πρωτοποριακή μέθοδο που συνδιάζει μετρήσεις Σπανίων Γαιών (REE) και κοσμογενών ισοτόπων ^{36}Cl πάνω στην σεισμικά αποκαλυμμένη επιφάνεια του ρήγματος. Η ανάλυση των δεδομένων δείχνει ότι το ρήγμα είναι ενεργό και έχει φιλοξενήσει τουλάχιστον 5 μεγάλου-μεγέθους σεισμούς τα τελευταία 16000 χρόνια. Οι δύο πιο πρόσφατοι σεισμοί έλαβαν χώρα 200 και 400 χρόνια πριν από σήμερα και άθροισαν συνολικά 3.5 μέτρα σεισμικής μετατόπισης. Η χρονολογία των παλαιότερων 3 σεισμών προσδιορίσθηκε στα 8200, 15000 και 16000 χρόνια πριν από σήμερα με σεισμικές ολισθήσεις 2.5, 1.2 και 1.8 μέτρα, αντίστοιχα. Από το μέγεθος των σεισμικών ολισθήσεων συμπεραίνουμε ότι το μέγεθος των σεισμών που προκλήθηκαν από το ρήγμα του Σπηλίου κυμάνθηκε από M 6.3-7.3 ενώ ο μέσος ρυθμός επανάληψης τους είναι ~3500 χρόνια. Τα παραπάνω δεδομένα αποκαλύπτουν ότι το ρήγμα του Σπηλίου όχι μόνο δεν έδρασε κατά την Μινωϊκή περίοδο αλλά, αντιθέτως, την περίοδο αυτή πέρασε μια μακροχρόνια φάση σεισμικής 'ηρεμίας'. Συνεπώς η μελέτη μας απορρίπτει την υπόθεση ότι το ρήγμα του Σπηλίου ευθύνεται για την καταστροφή της Μινωϊκής Φαιστού, παρά το γεγονός ότι σήμερα είναι ένα από τα πιο ενεργά ρήγματα στην Κρήτη. Το υπεύθυνο για τις καταστροφές ρήγμα παραμένει λοιπόν υπό αναζήτηση και εδώ προτείνουμε δύο νέα υποψήφια ρήγματα.

INTRODUCTION: Earthquakes are one of the deadliest natural disasters. About 20% of the Earth's population lives in areas of seismic hazard. Every year, there are approximately 150 large (>6M) earthquakes worldwide, causing an average of 20,000 casualties since the beginning of the 20th century and significantly impacting the economies and the sustainable development of the affected societies. The death toll in Europe alone during the last 500 years exceeds half a million, whilst the associated economic loss in just the last century exceeds €54 billion (European Geotechnical Network for Research and Development, 2005). Therefore, better understanding and forecasting of earthquake occurrence is one of the most pressing humanitarian goals within the sciences.

Tectonic faults are breaks in the Earth's crust that grow primarily due to large magnitude earthquakes (Stein et al., 1988). Over millions of years, large cumulative displacements (e.g. >5km) accrue on faults as a result of 100's to 1000's of earthquakes; however, the systematics of this process is poorly understood. This is mainly due to the brevity of the available instrumental and/or historic earthquake record in comparison to the repeat times of large earthquakes on most faults globally. *Paleoseismological investigations* (i.e. fault trenching, etc.) are capable of extending the instrumental and/or historic earthquake record by including the majority of surface rupturing prehistoric earthquakes of M>6 on any particular fault (Fig. 1) (McCalpin, 1996). The identification of the timing between, and slip during, successive earthquakes on individual faults is vital in earthquake research as it highlights, and to some extent constrains, the

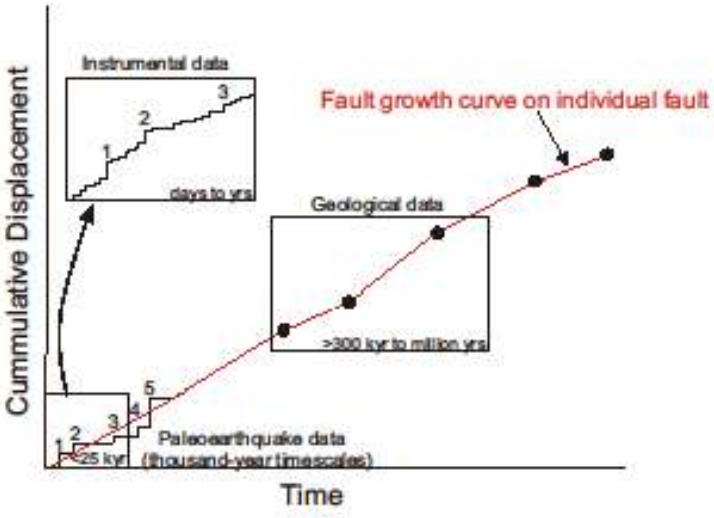

Figure 1: Schematic diagram illustrating fault-slip accumulation over instrumental (days to yrs), paleoearthquake (e.g., <25 kyr) and geological (e.g., >300 kyr) timescales. Numbered steps in the paleoearthquake data represent large ground-surface rupturing earthquakes while steps in the day-to-year long data represent small-sized instrumentally recorded earthquakes. Data resolution increases with decreasing timescales. Modified from Mouslopoulou et al., 2009.

variability associated with the complex phenomenon of earthquake occurrence (Nicol et al., 2009). Thus, *paleoseismology* increases the time-window over which earthquake information is available to thousands of years, providing a more realistic estimate of the seismic hazard of a particular fault (Fig. 1).

AN INTRODUCTION ON HOW EXHUMED FAULT SCARPS MAY RECORD PAST EARTHQUAKE ACTIVITY: During a large earthquake, a portion of a normal fault plane that was previously buried is suddenly exposed to the atmosphere. As further large earthquakes occur, the exposed fault plane becomes progressively larger and the succession forms a topographic escarpment, the height of which can be attributed to a number of past earthquakes (Benedetti et al., 2002). If we could identify the sections of the scarp that became successively exposed through time, we would know the number and size of the earthquakes generated by this fault. Accordingly, if we could date those sections, then we would know the timing of each earthquake.

In the case of *limestone* fault scarps the number, size and timing of earthquakes may indeed be constrained. As a section of a normal fault plane is suddenly exhumed, it becomes exposed to supergene weathering (rain, wind, vegetation and bacterial activity) and cosmic radiation (secondary neutrons and muons interact with Ca of the limestone scarp). The longer the surface is exposed, the more intense the weathering and the absorption of cosmic radiation. It is known that differential weathering of limestone scarps may be recorded in the chemical content of Rare Earth Elements (REE) (Manighetti et al., 2010; Mouslopoulou et al., 2011). Specifically, the concentration of REE generally decreases up-scarp, and peaks at sections of the scarp where the limestone was in direct contact with the paleosol (the limestone becomes enriched in REE while buried below the upper soil). Thus, a fault scarp is expected to include a series of rupture zones which have been weathered and exposed to radiation over significantly different time spans. The degree of weathering will reveal the number and size of the earthquakes, whereas the cosmic radiation will constrain their timing.

RESEARCH OBJECTIVES: The *primary* research objective of this study is to constrain the paleoearthquake history on the Spili Fault, a normal fault located in central Crete (Fig. 2), and assess whether movement on this fault relates to the destruction of the nearby Minoan Palace of Phaistos.

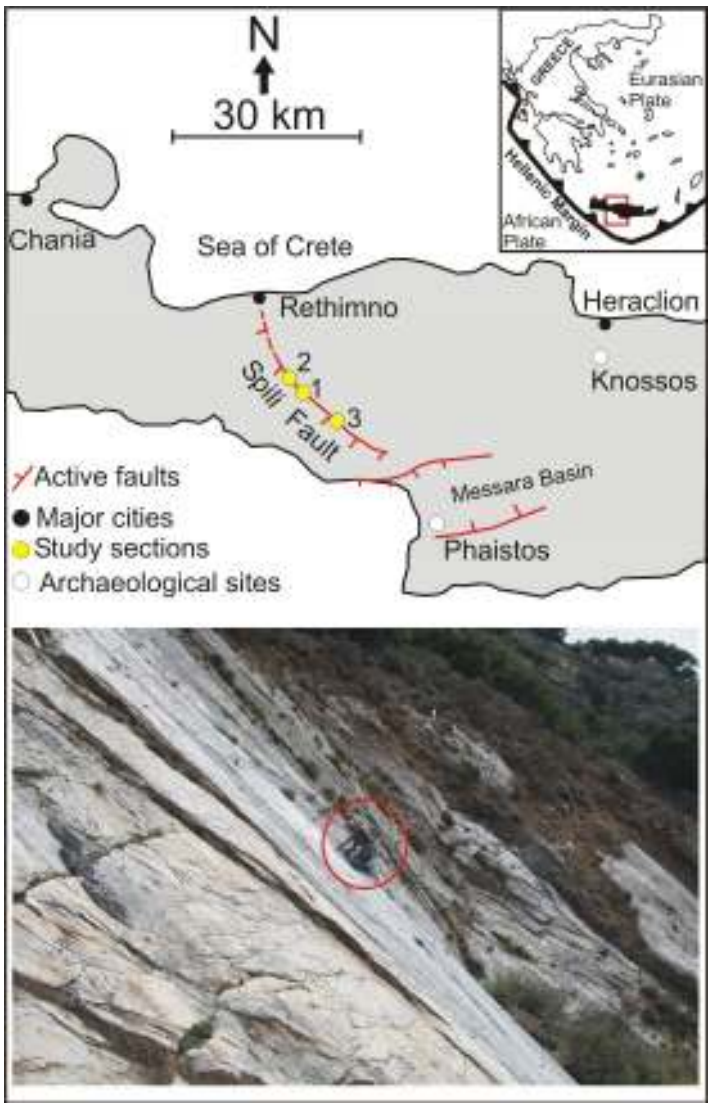

Figure 2: Schematic map of the Spili Fault traversing central Crete. The study sites are indicated by yellow circles. 1=Spili, 2=Health Center, 3=Platanes. The main modern and ancient cities are also indicated.

RESEARCH METHODOLOGY: To accomplish the primary objective we performed paleoseismological investigations along the Spili Fault in central Crete. In order to identify the number, size and timing of the large-magnitude prehistoric earthquakes that ruptured this normal fault, we employed a globally novel technique that involves a) identification and measurement of the *Rare Earth Elements (REE)* hosted in the exhumed limestone fault scarp; b) measurement of the *in situ cosmogenic* ^{36}Cl on each rupture zone. The former technique will provide the number and size of the earthquakes whereas the latter, the timing of the earthquakes. Specifically, paleoearthquake investigations involved 4 individual steps:

Step 1: *Sampling of exhumed limestone fault scarps for REE analysis (Fieldwork-A)*

Once the appropriate section was selected (Site-1), a total of 54 limestone core-samples were extracted from the exhumed fault plane in an upscarp direction, every 30 cm. Each

core-sample was 4 cm long and 2cm wide. Four samples were also extracted below the soil surface, down to depth of -0.7 m.

Figure 3: Sampling the lower 15 m of the Spili Fault at Site-1 for REE analysis (a) and the lower 9 m at Site-2 for cosmogenic dating (b) using a portable drill and rock-saw, respectively.

Step 2: *Identification and measurement of REE (Lab analysis-A)*

This stage involved the following individual steps per limestone core-sample: removal of 2mm core coating, 2cm core slicing, manual core crashing down to less than sugar grain-size, digestion of limestone grains aided by a series of acids (chemical preparation stage), centrifugation of the solutions and finally measurement of the content of REE on each sample by Inductively Coupled Plasma Mass Spectrometry (ICP-MS) equipment.

The digestion of the limestone grains (chemical preparation stage) was achieved through the following individual steps:

a) Initial dissolution with HCl until dryness for carbonates removal;

b) Dilution with HNO_3;

c) Dissolution with a mixture of HF, HNO_3 HCl and digestion in microwave;

d) Addition of EDTA and second digestion in microwave;

e) Dryness and dilution with HNO_3.

This analysis provided the number and size of the earthquakes on each fault. This analysis took place at the Department of Environmental Engineering at the Technical University of Crete (laboratory: Hydro-geochemical engineering and remediation of soils).

Step 3: *Cosmogenic Isotope sampling (Fieldwork-B)*

During this stage we extracted limestone-samples for ^{36}Cl cosmogenic dating of the identified, during the previous stage, earthquakes. Specifically, we used an electric rock grinder to remove a 15cm wide and 3cm thick section of the entire exhumed limestone fault plane. This technique is used routinely for cosmogenic isotope dating. During this stage we extracted a total of 208 samples for ^{36}Cl cosmogenic dating of the earthquakes. Specifically, we extracted 106 samples from the Site 1, 82 samples from Site 2 and 20 samples from Site 3.

Step 4: *Cosmogenic dating of prehistoric earthquakes (Lab analysis-B)*

The last step concerns the dating of each identified earthquake by determining the concentration of ^{36}Cl as a function of scarp height. ^{36}Cl is produced primarily through interaction of cosmic rays with Ca within the calcite ($CaCO_3$) of the limestone scarp. Because the production rate of ^{36}Cl and its distribution below the surface are known, the concentration of cosmogenic ^{36}Cl can be used to calculate how long a surface has been exposed to cosmic radiation. This analysis took place at the laboratory facilities of CNRS in France (Université Aix-Marseille III), in collaboration with Dr. Lucilla Benedetti, an internationally recognised expert in cosmogenic dating. Dr Mouslopoulou paid a fortnight visit at CEREGE to actively participate in the chemical analysis.

This analysis included the following individual steps: a) sample preparation for chemical Cl extraction, b) Accelerator Mass Spectrometry (AMS) measurements and ^{36}Cl concentration determination, c) analysis of host rock chemical composition, d) analysis of colluvial wedge chemical composition and e) determination of the density of the fault scarp rocks and colluvium (Schlagenhauf et al., 2010).

The final measurements of ^{36}Cl concentrations provided the timing of each earthquake.

Some information about the rock sampling and crushing:

Sampling in all cases involved extraction of carbonate rock from near-vertical (~75-80°) fault-scarps. The equipment used included an electrical generator, portable drill or rock-saw, chisel, hammer and climbing equipment (Figs 3 & 4a). Following the extraction, we manually crushed (inside an agate mortar) the REE samples, after having removed the upper 2mm of the outer core coating (Fig. 4b). Each core required about 40 minutes of manual crushing. We also crushed down to sugar-grain size using an electrical mill a total of 91 limestone slabs for ^{36}Cl analysis. Each slab required about 30 minutes. Subsequently we used a sheave to separate fractions of the crushed material (the ^{36}Cl content is measured on carbonate grain-sizes ranging from 250 to 500μm).

Figure 4: (a) Sampling the lower 2m of the Spili Fault at Site-3 for cosmogenic dating; (b) Prior to the chemical treatment stage, carbonate cores extracted for REE analysis were manually crushed down to sugar grain size within an agate mortar.

RESULTS: We successfully mapped the entire surface trace of the Spili Fault (~20 km) and identified three sections for sampling and subsequent analysis: the 'Spili' or Site-1, the 'Health Centre' or Site-2 and 'Platanes' or Site-3 (see yellow circles in Fig. 2). This plan is somewhat different to the one originally proposed, where we were to analyse data from Site-1 only. Despite the fact that including two new sites involved significant additional work, that proved to be crucial for recovering the slip history on the Spili Fault as the ^{36}Cl measurements that derived from Site-2 were more robust compared to Site-1. Specifically, by combining REE measurements from the lower 15 m at Site-1 with ^{36}Cl measurements from the lower 9 m at Site-2 we recovered a minimum of seven paleoearthquakes that were accommodated by the Spili Fault and constrained the timing on the five most recent of these events.

The ^{36}Cl measurements from Site-1 are sparse and of low-concentration and thus difficult to interpret. The ^{36}Cl measurements from Site-3 are, up to date, inconclusive. For these reasons the above data are not included in the subsequent analysis and the timing of the identified earthquakes is based on measurements from Site 2.

NUMBER, SIZE AND TIMING OF PAST EARTHQUAKE ACTIVITY ON THE SPILI FAULT: Seven paleoearthquakes have been identified to have ruptured the Spili Fault, the most recent five of which occurred during the last 16000 years. In the following sections, we discuss how individual earthquakes may be constrained on a fault scarp by combing the REE method with cosmogenic (^{36}Cl) dating.

RARE EARTH ELEMENTS (REE) ANALYSIS: In order to constrain the number and size of the past earthquakes that ruptured the Spili Fault we measured the REE content at 54 upscarp localities at Site-1 (Table 1). In Figure 5, where a concentration measure ($\Delta i/\Delta m$) is plotted as a function of fault scarp height, we explore the upscarp concentration evolution for each of the REE. Specifically, the Y-axis in Figure 5 measures the difference (Δi) between a given concentration of an element (i) in core (Ci) and the mean concentration (Cm) of the same element over the entire fault scarp collection (Δi=Ci-Cm),

Table 1: Table illustrates the REE measurements (in ppm) as a function of their sampling position along the height of the scarp (-0.5 to 15.4 m) at Site-1.

Scarp Height (m)		-0.5	-0.2	0.1	0.4	0.7	1	1.3	1.6	1.9	2.2	2.5	2.8	3.1	3.4	3.7	4
Y-REE concentrations (ppm)	Y	1.681	1.564	1.530	0.730	0.878	0.955	1.165	1.098	0.994	1.655	1.994	2.910	2.064	2.126	2.276	1.253
	La	0.913	0.969	0.952	0.506	0.616	0.670	0.751	0.889	0.462	0.890	0.814	1.056	0.836	0.947	0.915	0.662
	Ce	1.396	2.746	2.480	0.726	1.627	0.956	1.290	1.270	0.813	1.654	2.374	2.090	1.689	2.705	2.139	1.437
	Pr	0.188	0.211	0.215	0.124	0.136	0.150	0.158	0.184	0.092	0.202	0.201	0.266	0.228	0.234	0.200	0.157
	Nd	0.697	0.765	0.797	0.413	0.438	0.521	0.617	0.716	0.374	0.732	0.703	0.902	0.771	0.798	0.645	0.588
	Sm	0.169	0.189	0.191	0.102	0.120	0.124	0.145	0.149	0.094	0.177	0.206	0.253	0.230	0.216	0.180	0.164
	Eu	0.071	0.067	0.069	0.037	0.042	0.046	0.048	0.051	0.038	0.057	0.057	0.076	0.061	0.062	0.053	0.048
	Gd	0.275	0.297	0.283	0.145	0.173	0.188	0.210	0.221	0.145	0.243	0.254	0.305	0.253	0.263	0.235	0.207
	Tb	0.049	0.051	0.053	0.030	0.036	0.036	0.035	0.032	0.026	0.040	0.038	0.053	0.040	0.039	0.038	0.029
	Dy	0.238	0.241	0.246	0.144	0.165	0.168	0.176	0.155	0.130	0.199	0.212	0.275	0.216	0.206	0.190	0.187
	Ho	0.049	0.054	0.049	0.029	0.034	0.035	0.035	0.032	0.031	0.039	0.035	0.051	0.035	0.032	0.031	0.030
	Er	0.187	0.203	0.210	-	0.102	-	0.111	0.094	0.094	0.128	0.127	0.182	0.129	0.140	0.115	0.120
	Yb	0.089	0.101	0.096	0.059	0.069	0.066	0.062	0.033	0.044	0.074	0.083	0.119	0.081	0.076	0.069	0.063
	Lu	0.011	0.011	0.012	0.007	0.008	0.008	0.006	0.002	0.009	0.007	0.005	0.007	0.003	0.002	0.003	0.001

4.3	4.6	4.9	5.2	5.5	5.8	6.1	6.4	6.7	7	7.3	7.6	7.9	8.2	8.5	8.8	9.1	9.4	9.7
1.845	1.750	1.690	1.645	1.999	0.874	0.697	1.011	1.008	2.074	2.789	1.401	0.834	0.907	0.743	1.112	1.148	0.556	0.461
1.004	0.906	0.916	0.701	0.956	0.447	0.326	0.348	0.420	0.833	1.372	0.530	0.349	0.347	0.282	0.480	0.387	0.214	0.199
2.102	2.054	2.242	1.462	1.929	0.758	0.610	0.677	0.809	1.374	2.005	1.158	0.659	0.600	0.410	0.709	0.515	0.541	0.342
0.277	0.238	0.235	0.182	0.245	0.103	0.073	0.081	0.098	0.186	0.236	0.091	0.056	0.055	0.046	0.077	0.056	0.036	0.034
1.035	0.899	0.884	0.668	1.010	0.414	0.286	0.322	0.382	0.725	0.892	0.291	0.186	0.172	0.141	0.245	0.187	0.104	0.105
0.294	0.260	0.259	0.195	0.310	0.112	0.074	0.095	0.103	0.182	0.213	0.070	0.043	0.039	0.034	0.059	0.048	0.021	0.021
0.098	0.080	0.077	0.061	0.099	0.037	0.022	0.028	0.031	0.061	0.078	0.021	0.014	0.010	0.008	0.018	0.011	0.004	0.003
0.348	0.306	0.301	0.240	0.381	0.148	0.105	0.138	0.141	0.239	0.294	0.110	0.071	0.068	0.049	0.089	0.074	0.032	0.032
0.053	0.046	0.044	0.038	0.059	0.023	0.015	0.024	0.022	0.032	0.039	0.016	0.010	0.010	0.006	0.013	0.011	0.003	0.003
0.320	0.281	0.265	0.233	0.384	0.154	0.106	0.157	0.142	0.202	0.247	0.091	0.061	0.057	0.047	0.078	0.071	0.031	0.029
0.055	0.051	0.045	0.041	0.076	0.028	0.019	0.029	0.027	0.039	0.048	0.015	0.008	0.006	0.004	0.013	0.009	0.001	0.001
0.166	0.227	0.466	0.121	0.218	0.083	0.136	0.220	0.198	0.102	0.127	0.300	0.098	0.068	0.033	0.053	0.043	0.195	0.022
0.107	0.098	0.086	0.080	0.143	0.056	0.038	0.049	0.049	0.059	0.070	0.032	0.021	0.022	0.014	0.026	0.021	0.013	0.014
0.006	0.006	0.004	0.003	0.014	0.003	0.002	0.003	0.003	0.006	0.007	-	-	-	-	-	-	-	-

10	10.3	10.6	10.9	11.2	11.5	11.8	12.1	12.4	12.7	13	13.3	13.6	13.9	14.2	14.5	14.8	15.1	15.4
0.368	0.893	0.694	0.594	1.849	2.830	1.703	2.087	2.285	2.135	0.502	0.358	0.855	1.192	1.086	3.271	5.901	5.009	3.939
0.180	0.392	0.270	0.243	1.292	2.036	0.614	0.772	0.866	0.784	0.206	0.159	0.288	0.331	0.293	1.034	2.378	2.032	1.549
1.702	0.757	1.494	1.542	4.154	5.245	4.864	2.995	2.862	2.833	0.872	2.953	2.550	1.007	1.245	2.238	6.284	4.977	4.526
0.038	0.046	0.022	0.043	0.227	0.344	0.027	0.063	0.089	0.076	0.049	0.048	0.007	0.015	0.051	0.131	0.473	0.403	0.293
0.124	0.241	0.167	0.139	0.839	1.233	0.317	0.393	0.455	0.410	0.116	0.126	0.164	0.197	0.163	0.601	1.787	1.541	1.238
0.032	0.047	0.040	0.033	0.131	0.202	0.076	0.085	0.063	0.045	0.037	0.037	0.039	0.052	0.040	0.094	0.390	0.340	0.262
0.012	0.014	0.016	0.015	0.035	0.060	0.032	0.032	0.038	0.028	0.012	0.015	0.016	0.018	0.018	0.050	0.093	0.087	0.049
0.055	0.066	0.064	0.057	0.180	0.305	0.161	0.155	0.177	0.131	0.048	0.070	0.076	0.075	0.068	0.246	0.658	0.592	0.454
0.005	0.009	0.007	0.007	0.025	0.038	0.019	0.022	0.026	0.021	0.006	0.006	0.009	0.012	0.011	0.038	0.047	0.045	0.063
0.034	0.054	0.046	0.040	0.124	0.215	0.106	0.115	0.137	0.109	0.034	0.033	0.053	0.064	0.059	0.228	0.561	0.527	0.385
0.006	0.011	0.009	0.008	0.026	0.038	0.022	0.023	0.028	0.023	0.006	0.006	0.010	0.013	0.012	0.005	0.065	0.056	0.020
0.021	0.033	0.030	0.029	0.080	0.133	0.070	0.078	0.093	0.079	0.024	0.026	0.041	0.047	0.045	0.148	0.376	0.342	0.252
0.019	0.023	0.028	0.028	0.068	0.100	0.053	0.054	0.057	0.047	0.022	0.029	0.033	0.034	0.036	0.059	0.210	0.201	0.144
0.0003	0.001	0.001	0.002	0.008	0.012	0.004	0.005	0.005	0.004	-	0.0004	0.002	0.002	0.002	0.007	0.020	0.019	0.015

normalized to the mean absolute value of those differences (*Δm)*. Data reveal a nearly linear decrease of the average REE-Y concentration with increasing scarp height (dashed line in Fig. 5). The average depletion rates of the L-REE and H-REE on the Spili Fault scarp are 8.5 %/m and 10.6 %/m, respectively, while for the entire REE-Y population, it is ca. 9.3 %/m.

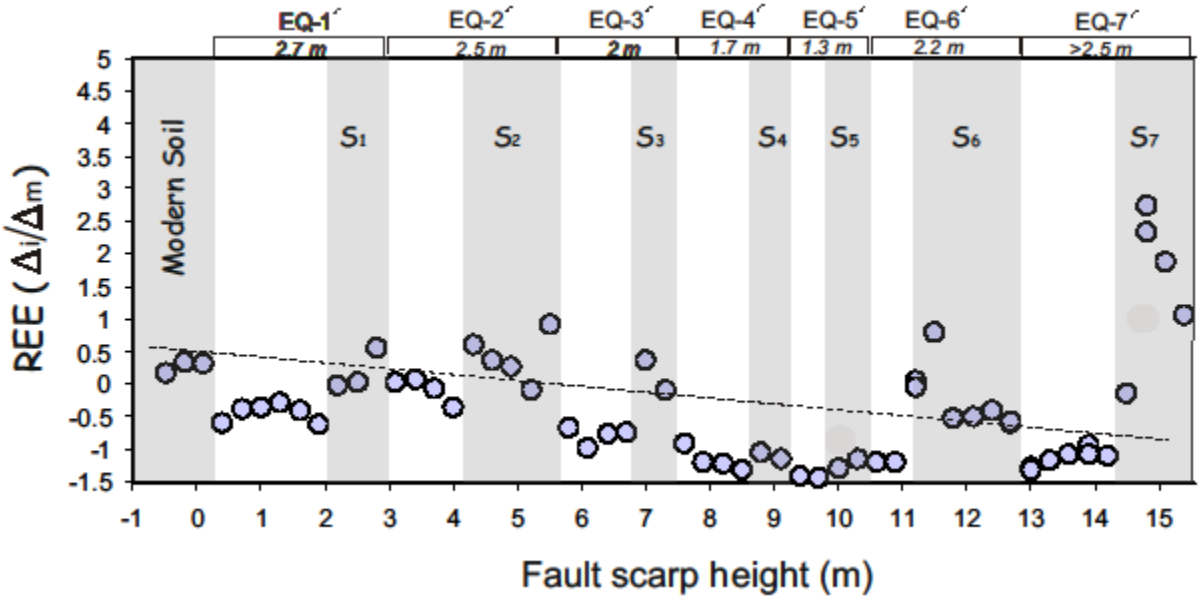

Figure 5: Plot showing the variability in the concentration of the REE as a function of sample position along the fault scarp. The Y-axis measures the difference Δi between a given concentration in core i (Ci) and the mean concentration (Cm) over the entire fault scarp collection (Δ*i*=C*i*-Cm), normalized to the mean absolute value of those differences (*Δm)*. Circles correspond to the average value of 14 different REE at each locality. Domains *Si*, which are shaded grey, indicate scarp sections enriched in REE. Dashed line indicates the decreasing trend (depletion) of the average *Δi/Δm* with increasing scarp height.

The most striking feature illustrated in Figure 5 is that, superimposed on the overall depleting trend upscarp, there is a continuous and clear signal of fluctuations in the REE concentrations as a function of fault scarp height. In detail, there are domains in which the REE concentrations are locally increased. These domains, which are highlighted by grey shading in Figure 5 are always preceded or followed by scarp sections which are characterised by lower concentrations in REE. For example, the section of the fault scarp that is currently buried up to 0.5 m below the ground surface has, on average, 60% higher REE-Y concentration compared to the section of the scarp immediately above the ground surface (Fig. 5). The 60% 'drop' in the concentration persists up to the height of about 2m, where another increase of ca. 75% in the REE concentration occurs (Fig. 5). Overall,

our data record a minimum of seven, such *'fluctuations'* in the concentration of REE up the 15m of the Spili Fault plane (Fig. 5).

According to the model presented in earlier studies (Manighetti et al., 2010; Mouslopoulou et al., 2011), each concentration fluctuation is associated with an earthquake event that instantly exhumed subaerially sections of the fault scarp with depleted and elevated REE concentrations. Thus, we have identified a minimum of seven such paleoearthquakes the size of which ranges from 1.3 to 2.7 m.

COSMOGENIC (^{36}Cl) DATING OF EARTHQUAKES: We measured and modelled the content of *in situ cosmogenic ^{36}Cl* on 41 limestone samples extracted from the lower 9 m of the fault scarp at Site-2 (Table 2, Fig. 6). The total scarp height at this locality is about 12-13 m.

The modelling of the ^{36}Cl results has taken into account the dip of the fault at Site-2, the density and the dip of the alluvial fan, the dip of the older scarp section (above the sampling site) and the shading that may be induced locally by the surrounding topography (Schlagenhauf et al., 2010).

Results indicate that the lower section (~3.5 meters) of the fault scarp is much younger than the remaining scarp. Examination of the graph in Figure 6 reveals two sharp discontinuities at 1 and 3.5 meters along the height of the scarp. These discontinuities are interpreted to result from at least two large magnitude earthquake events. The timing of these earthquakes is modelled to be at 200 and 400 years BP, respectively. Following, at about 6m upscarp, there is another discontinuity, dated at ~8200 years B.P. The large time-lag between the second and third identified earthquakes on the Spili Fault is reflected in the increased content in ^{36}Cl at six meters compared to the content measured lower on the scarp (the upper section of the scarp has been exposed to cosmic ray radiation for longer time-periods than the lower section of the scarp). This is also evident in the field, when one compares the roughness of the fault plane at different localities upscarp. Following, the 4th and 5th recorded discontinuities (earthquakes) are identified at

7.2 m and 9 m upscarp and their timing is modelled at 15000 and 16000 years BP, respectively (Fig. 6).

The slip-sizes of the five most recent earthquakes identified at Site-2 (starting from the most recent: 1m, 2.5m, 2.5m, 1.2m and 1.8) are overall comparable to those derived from Site-1 by the REE method (starting from the most recent: 2.7m, 2.5m, 2m, 1.7m and 1.3m). Lateral slip variability is commonly observed along faults, even over short lateral distances. In our case the two sites are located ~2 km apart and the slip variability observed is not surprising (perhaps with the exception of the most recent event).

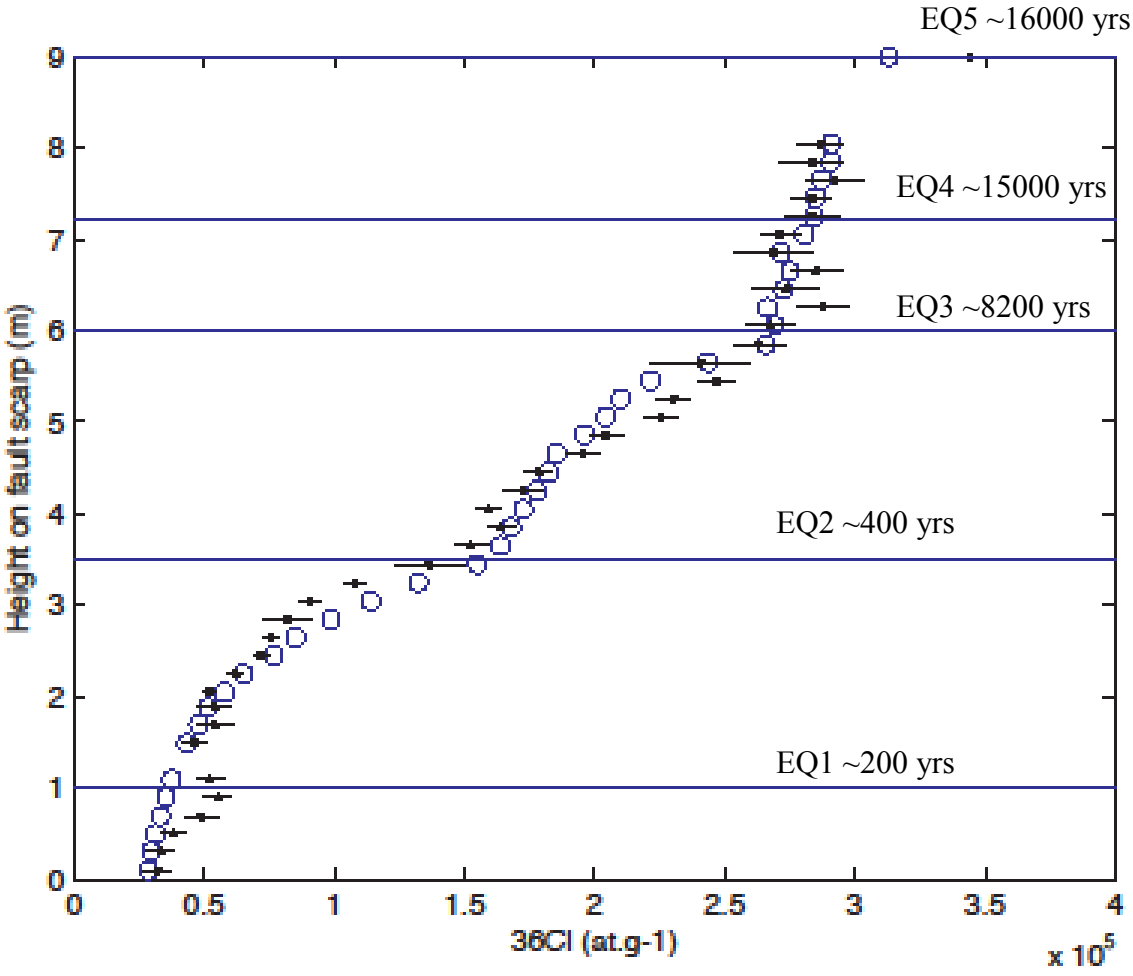

Figure 6: Modelling (hollow circles) of the ^{36}cl concentrations (black circles) that derive from the lower 9m of the Spili Fault at Site-2. Each line represents a discontinuity interpreted to result from at least one paleoearthquake. The discontinuities (earthquakes) are indicated by horizontal lines. The timing of each earthquake is indicated on the graph.

Table 2: Table illustrates the ^{36}Cl measurements (in at/g.rock), along with their uncertainties, as a function of their sampling position along the height of the scarp (0-9 m) at Site-2.

Upscarp locality	[36Cl] AMS	Uncertainty	Upscarp locality	[36Cl] AMS	Uncertainty
cm	at/g.rock		cm	at/g.rock	
10	32113	5520	425	172477	7041
30	33502	5393	445	178675	5020
50	38131	4762	465	195647	5868
69	49140	6023	485	204573	6468
89	55156	5576	505	225649	6218
109	52410	5146	525	230347	6127
129		5861	545	246929	6523
149	46352	5020	565	240763	18805
169	54215	6724	585	263236	9833
188	54012	6223	605	267700	9290
205	52289	2410	625	287788	10090
225	62223	2897	645	273602	12382
245	72001	3124	665	285345	9379
265	75619	3032	685	268896	15182
285	82338	9326	705	271381	7488
305	90727	3627	725	283715	10649
325	108039	3494	745	283520	7661
345	136640	13159	765	292442	11100
365	152708	6020	785	283710	12174
385	164272	5238	805	286884	8553
405	159338	4951	900	344225	15245

RELATION BETWEEN MOVEMENT ON THE SPILI FAULT AND THE DESTRUCTION OF PHAISTOS: Despite the fact that the Spili Fault proved to be one of the most active faults on the island of Crete, having accommodated two large magnitude earthquakes over the last 400 years, it seems to have no apparent relation to neither of the destructions that occurred at the Palace of Phaistos during the Minoan period. This is because our data show that the fault has not produced any large, surface rupturing, earthquake during an approximately 7000 year-long period, from ~400 to ~8200 yrs BP. The double destruction of Phaistos was dated by archaeologists to be at ~3400 and 3750 yrs BP (Monaco and Tortorici, 2004).

By contrast, recent movement on the Spili Fault (200 and 400 years BP) can be associated with historic earthquakes. In detail, the two recent earthquakes identified on the Spili Fault can be correlated with severe shaking recorded on the island by travellers, observers, priests and writers in late16th and early 19th centuries (Papadopoulos, 2011). Specifically, the older earthquake (400 years BP) may be associated with the large November 16, 1595 earthquake that destroyed Chania and Rethymnon and killed a number of people. Historic sources assess the magnitude of this earthquake as M6.4 in the Richter scale. The younger earthquake (200 years BP) may be associated with the destructive earthquake of June 21st, 1805 that was severely felt at Chania and Rethymnon. Its magnitude was estimated to be M7 in the Richter scale (Papadopoulos, 2011).

Now concerning the mystery associated with the destruction of Phaistos by earthquakes, other candidate faults may be the nearby Ag. Triada and Klima faults. Despite the fact that these faults look less active than the Spili Fault, they are clearly active, as they form triangular facets and displace alluvial fans. The Ag. Triada and Klima faults are located 2 and 5 km from Phaistos, respectively.

IMPLICATIONS FOR SEISMIC HAZARD: The Spili Fault is one of the most active faults on Crete. It has accrued 9 m of displacement over a period of 16000 years. Based on these measurements, the slip rate (SR) on the fault is ~ 0.6 mm/yr.

Each identified earthquake on the Spili Fault produced co-seismic slip that ranged from 1.2 to ~2.7 m. Using the Wells and Coppersmiths equation M=6.69+0.74*log(MD), where MD is the Maximum Displacement per earthquake event, we derive earthquake magnitudes ranging from M 6.3-7.3.

Earthquakes of that magnitude may be highly damaging. Therefore it is important to discuss the frequency with which large magnitude earthquakes are accommodated by the Spili Fault. To achieve this, we introduce a term called 'earthquake recurrence interval'. The earthquake recurrence interval (RI) is the period of time between large magnitude events on an individual fault (McCalpin, 1996). The RI can be estimated using two different methods: 1) directly from the earthquakes observed on the fault-scarp (observed RI) or 2) calculated from the mean single event displacement (SED) and the slip rate on the fault (estimated average RI). The methods are independent from one another and collectively provide a powerful means of estimating recurrence intervals and their variability.

OBSERVED RI ON THE SPILI FAULT: Based on the timing of the five most recent earthquake events on the Spili Fault, that is 200, 400, 8200, 15000 and 16000 years BP, we derive the following four RI's: 200, 7800±200, 6800±200 and 1000±200.

Therefore, based on these observed time intervals, the average RI on the Spili Fault is ~3950 years.

CALCULATED RI ON THE SPILI FAULT: The value of "calculated average recurrence interval" is based on the cumulative displacement of a dated feature (fault-scarp in our case) that has been offset by multiple earthquakes. The slip per event (D) is typically estimated from the maximum or average slip documented during single earthquakes. The average D for the Spili Fault is 2m. Knowing that the slip rate (SR) on the fault is 0.6 mm/yr, we derive the calculated average recurrence interval based on the equation: $RI_{(calc)} = D/SR = 2000$ mm / 0.6 mm/yr ~ 3300 years.

The above data suggest that the calculated (~3300 year) average recurrence interval on the Spili Fault is, within uncertainties, comparable to that observed (~3950 years) on the fault by dating individual earthquakes. This is encouraging because it may suggest that our sampling window (e.g. 16000) is large enough to overcome the short-term variability that often arises when we sample fault activity that is not representative of the long-term fault's behaviour (e.g. temporally clustered earthquake events). For example, the observed RI on the Spili Fault would have been much shorter had we only sampled the two most recent earthquakes on the fault. Nevertheless, as earthquakes on faults rarely occur periodically, the numbers associated with the earthquake recurrence intervals on a fault should be treated only as averages (Mouslopoulou et al., 2009).

RAISING THE PUBLIC AWARENESS ABOUT EARTHQUAKES IN CRETE:

Dissemination of the results to the citizens of Crete, and particularly the residents of Rethymnon, is vital. To achieve this we aim to give public talks at the local communities of Spili and Rethymnon, during which we will explain in plain language the results of our study. In doing so, we hope to familiarize the public with the natural phenomenon of earthquakes and the fact that there is an active fault, capable of generating large-magnitude earthquakes, in their neighbourhood. We have already contacted the mayor of Spili and he has encouraged our initiative.

We also plan to create a 'Geosite' (Γεώτοπο) at Sites 1 and 2, where people could visit and see the signature of large earthquakes on the landscape. Large signs indicating the size and timing of individual earthquakes will be placed directly on the fault plane whereas at the foot of the scarp there will be signs describing the methods of identifying paleoearthquakes and the reasons for doing so. We hope that the Geosite will not only attract tourists but it will also act as a hub for schools and other educational centres.

INSPIRATION FOR FURTHER WORK

a) REE ENRICHMENT MECHANISM: The enrichment of fault scarp sections in REE has been attributed to their paleo-contact with the upper soil. However, the REE

enrichment mechanism has yet to be established and the factors that control the REE mobility have yet to be constrained. To achieve this we designed, and already started implementing, further research steps that would allow us to investigate the REE enrichment mechanism on the soil/rock interface.

In detail, we designed pot experiments that would allow us to simulate the soil/rock interaction at two different temperatures (25 and 15^{o} C) (Fig. 7). Furthermore, we designed batch laboratory experiments to identify the kinetics of the REE adsorption on the limestone surface. Isotherm studies and pH-edge tests have been also designed and preliminary results have been obtained.

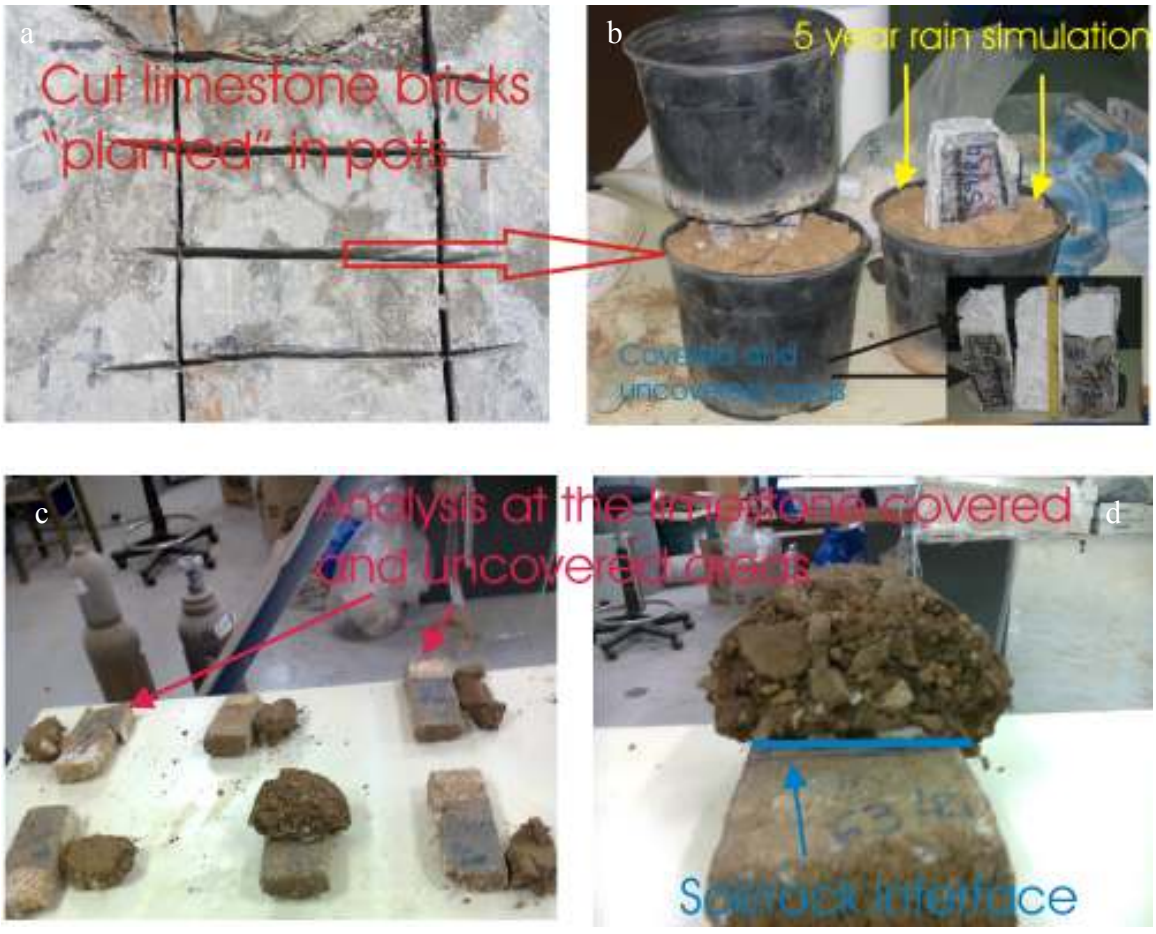

Figure 7: a) Limestone slabs extracted from the fault plane at Site-1 b) Irrigated "planted" slabs in pots with 5 years of rain simulation c) Slabs removed from the pots after the end of the simulation period; analysis was performed at both the covered with silicone and the 'free' sections of the slab.

In order to simulate the fault plane, we covered with silicone the entire slab apart from the face that represented the 'fault plane' (Fig. 7). Figure 8 shows the set-up of the pot experiment and the % change of the REE concentration after the simulation of 5 years of rainfall. Preliminary results show that there is an increase of the REE content in the 'fault-plane' (the uncovered) sections of the slab compared to the covered slab sections. This increase is decreasing towards greater depths in the pot and away from the soil interface (Fig. 8). Results also show higher enrichment of the Heavy-REE compared to the Light-REE at 25^{o} Celsius and generally lower increase of REE concentration at the temperature of 15 ^{o} Celsius.

The establishment and quantification of the REE enrichment mechanism on limestone faults is important because it will significantly improve our knowledge on the temporal resolution of individual paleoearthquakes on carbonate faults (e.g. we hope to quantify the minimum required time-intervals for the REE enrichment).

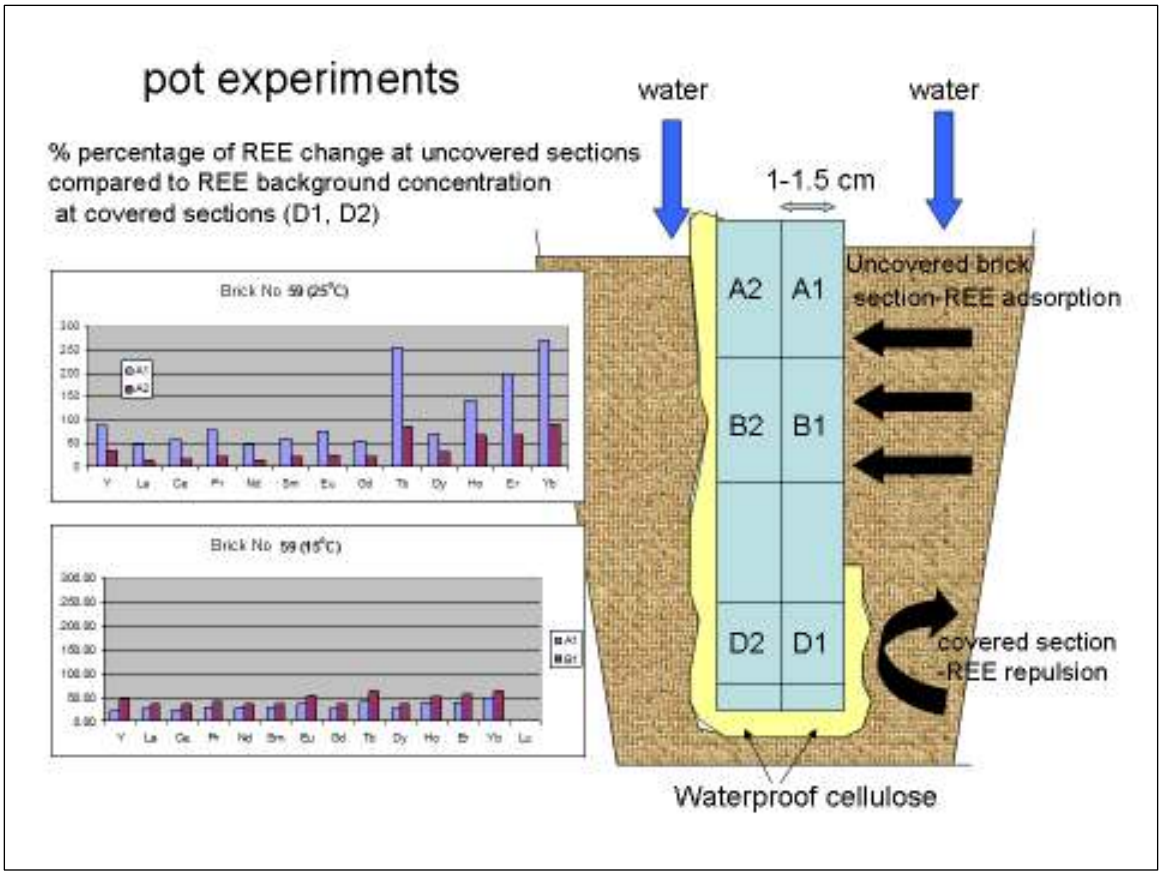

Figure 8: a) Pot experiment set-up and results of % of REE concentration change after 5 years rain simulation at two different temperatures.

b) IDENTIFY THE FAULT THAT DESTROYED PHAISTOS: We are keen to follow-up and resolve the mystery related to the destruction of Phaistos by earthquakes. We have identified two additional faults, those of Ag. Triada and Klima, which are active and are located within <5 km from the archaeological site of Phaistos. However, these faults are located within the basin of Messara and do not appear to displace carbonate rocks but younger Tertiary and Quaternary deposits. Therefore, they should be studied using different techniques (e.g. fault trenching) to those used in this study.

REFERENCES:

European Geotechnical Network for Research and Development, 2005. Determination of Socio-Economic Impact of Natural Disasters in Europe. FP5, GTC2-2000-33033, Contract G1RT-CT2001-05041, p.p., 1-173, ISBN 90 3760 495.

Benedetti L., Finkel, R., Papanastassiou, D., King, G., Armijo, R., Ryerson, F.J., Farber D., Flerit, F., 2002. Post-glacial slip history of the Sparta fault (Greece) determined by ^{36}Cl cosmogenic dating: evidence for non-periodic earthquakes. Geophysical Research Letters 29, 8701-8704.

Manighetti, I., Boucher, E., Chauvel, A., Schlagenhauf, A., Benedetti, L., 2010. Rare earth elements record past earthquakes on exhumed limestone fault planes. Terra Nova 22, 477-482.

McCalpin, J.P., 1996. Paleoseismology: San Diego, California, Academic Press, 588.

Monaco, C., Tortorici, L., 2004. Faulting and effects of earthquakes on Minoan archaeological sites in Crete (Greece). Tectonophysics 382, 103-116.

Mouslopoulou, V., Walsh, J.J., Nicol, A., 2009. Fault displacement rates on a range of timescales. Earth and Planetary Science Letters, 278, 186-197.

Mouslopoulou, V., Moraetis, D., Fassoulas, C., 2011. Identifying past earthquakes on carbonate faults: advances and limitations of the Rare Earth Element method based on analysis of the Spili Fault, Crete, Greece. Earth and Planetary Science Letters, 309, 45-55.

Nicol, A., Walsh, J.J., Mouslopoulou, V., Villamor, P., 2009. Earthquake histories and Holocene acceleration of fault displacement rates. Geology, 37, 911–914.

Papadopoulos, G., 2011. A seismic history of Crete, 0-416, Edition Oselotos, ISBN: 9789609499682

Schlagenhauf, A., Gaudemer, Y., Benedetti, L., Manighetti, I., Palumbo, L., Schimmelpfennig, I., Finkel, R., Pou, K., 2010. Using in-situ Chlorine-36 cosmo-nuclide to recover past earthquake histories on limestone normal fault scarps: A reappraisal of methodology and interpretations. Geophysical Journal International 182, 36–72.

Stein, R.S., King, G.C., Rundle, J.B., 1988. The growth of geological structures by repeated earthquakes: 2 Field examples of continental dip-slip faults. Journal of Geophysical Research, 93, 13319–13331.

Wells, D.L., Coppersmith, K.J., 1994. New empirical relationships among magnitude, rupture length, rupture width, rupture area and surface displacement. Bulletin of the Seismological Society of America, 8, 974-100.